The influence of mesoscale eddies on the detection of quasi-zonal jets in the ocean

Michael G. Schlax[1] and Dudley B. Chelton[1]

[1] Westward propagating Gaussian eddies with statistical characteristics estimated from altimeter observations but with purely random starting locations and times produce striated features in time-averaged maps of zonal velocity. The striations in these simulations have magnitudes and meridional scales comparable to those reported from time-averaged altimeter observations and model output in the central North Pacific and the California Current System. Time averages over the data records presently available are therefore not suitable for unambiguous detection of quasi-zonal jets. The presence of mapping error and background isotropic eddy kinetic energy also bias the regionally-averaged anisotropy of time averaged velocity fields, thus compromising the interpretation of anisotropy statistics. **Citation:** Schlax, M. G., and D. B. Chelton (2008), The influence of mesoscale eddies on the detection of quasi-zonal jets in the ocean, *Geophys. Res. Lett.*, *35*, L24602, doi:10.1029/2008GL035998.

1. Introduction

[2] Recent analyses of observations and ocean model output have revealed quasi-zonal striated features in fields of sea surface height (SSH) and zonal velocity [*Maximenko et al.*, 2008, and references therein]. These striations are generally interpreted as meridionally alternating zonal jets of the type predicted theoretically from 2-dimensional geostrophic turbulence theory [*Rhines*, 1975]. Unambiguous evidence for such jets would be an exciting confirmation of theory and would provide important insight into the dynamics of the mesoscale eddy field.

[3] Most of the analyses above rely upon long temporal averages. For the case of a 200-week average, *Maximenko et al.* [2005] conclude that the striations must be either relatively stationary features, such as jets, or the result of the time averaging of eddies following pathways defined by jets that are not readily apparent. The striations are generally more clearly defined where eddy variability is most energetic and the orientations of the striations are consistent with the dominant eddy propagation directions. The underlying assumption of *Maximenko et al.* [2005] is that the SSH and zonal velocity fields from randomly distributed eddies average to zero.

[4] Here we show that this assertion is not true. We present a simple model of Gaussian eddies with random starting locations and times, and with amplitudes, scales, lifetimes and generation rates conditioned by eddy statistics derived from altimeter observations. In simulated time-averaged fields, there is surprising persistence of striated features that could easily be mistaken for zonal jets.

[5] Another method for studying oceanic striations was proposed by *Huang et al.* [2007] who estimated the anisotropy of mid-ocean currents using altimeter data, ocean model output and simulated eddy fields [see also *Qiu et al.*, 2008; *Scott et al.*, 2008]. *Huang et al.* [2007] reported that nearly isotropic velocity fields in the North Pacific showed increasing anisotropy when time averaged and concluded that the observed anisotropy cannot be explained by propagating eddies alone. We will show that SSH mapping errors and the presence of isotropic non-eddy background signals can bias the regionally-averaged anisotropy sufficiently to account for the discrepancy between the observed and simulated anisotropies.

[6] These results do not disprove the existence of either zonal jets or of preferred eddy pathways. While sound physical reasons have been expounded for the existence of both, detection of jets in either the ocean or models is an extreme challenge because the O(1 cm s^{-1}) RMS jet velocities are generally more than an order of magnitude less than the RMS velocities associated with mesoscale eddies.

2. Statistics for Mesoscale Eddies

[7] The eddy statistics upon which our simulations are based were obtained from the locations of tracked eddies and estimates of their amplitude and scale [*Chelton et al.*, 2007, also Observations of westward-propagating sea surface height variability. Part 2: Space-time characteristics, manuscript in preparation, 2008]. Eddies were defined and tracked for the period 14 October 1992 through 3 January 2007 using the SSH fields constructed from merged altimeter data and distributed by AVISO (Archiving, Validation, and Interpretation of Satellite Oceanographic Data). The paths of eddies that were tracked in the North Pacific for ≥1 year are overlaid in Figure 1 on the track density based on eddies tracked for ≥16 weeks. Discussion of the apparent propensity for eddies to follow preferred pathways that is evident in Figure 1a and has been previously conjectured by *Maximenko et al.* [2005, 2008] and *Scott et al.* [2008] is deferred until section 5.

[8] The amplitude of each eddy is defined to be the difference between the SSH value on the contour enclosing the eddy and the peak SSH value within the contour. An "e-folding" scale is defined to be the radius of a circle with area equal to that within which SSH exceeds e^{-1} times the eddy amplitude. Because of discretization of the contours of SSH used to define eddy perimeters, these estimates of amplitude and e-folding scale are necessarily biased somewhat low (Chelton et al., manuscript in preparation, 2008).

[1]College of Oceanic and Atmospheric Sciences, Oregon State University, Corvallis, Oregon, USA.
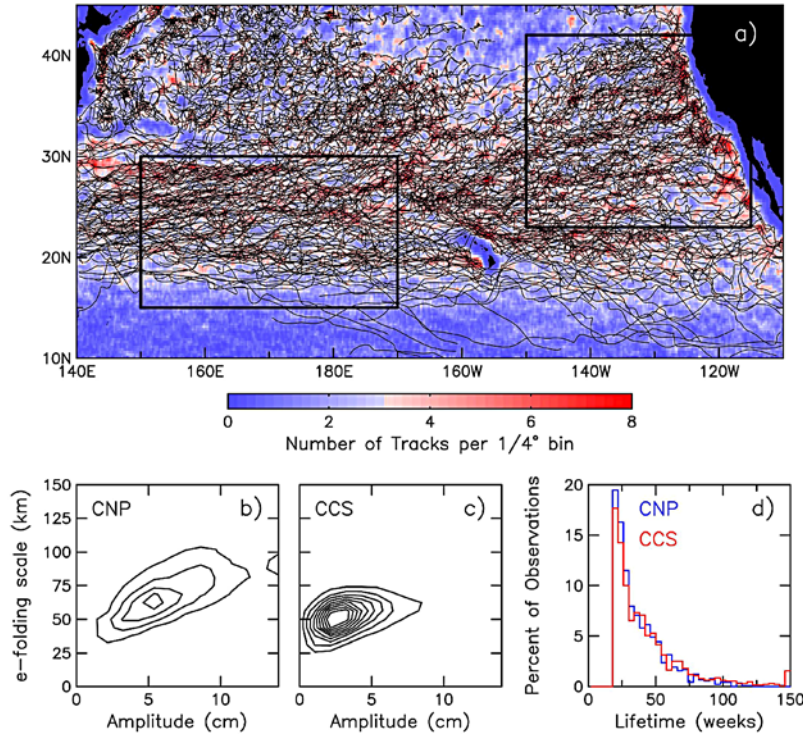
Figure 1. (a) Eddy tracks in North Pacific Ocean with lifetimes of ≥1 year overlaid on the number of tracks with lifetimes of ≥16 weeks crossing each 1/4° bin from 14 October 1992 through 3 January 2007. The rectangles delineate the Central North Pacific (CNP) and California Current System (CCS) regions considered in this study. (b and c) Two-dimensional histograms of eddy e-folding scale and amplitude and (d) histograms of eddy lifetimes for the CNP (blue) and CCS (red).

[9] The distributions of eddy amplitudes, scales and lifetimes shown in Figures 1b, 1c, and 1d for the Central North Pacific (CNP, 150E–170W, 15N–30N) and the California Current System (CCS, 150W–115W, 23N–42N) are based on eddies that were tracked for ≥16 weeks. These amplitudes and scales are the individual averages over all time steps of each tracked eddy. In both regions, the numbers of cyclonic and anticyclonic eddies are very nearly equal, and the distributions of amplitudes and scales for the two polarizations are very similar.

[10] The amplitudes and scales of the 878 eddies in the CNP are strongly correlated, have mean values of about 7 cm and 70 km, and are skewed towards values near 10 cm and 75–100 km. The 1268 eddies in the CCS have amplitudes and scales that are less strongly correlated and skewed, and have mean values of about 4 cm and 50 km. Eddy lifetimes (Figure 1d) have mean values of 35 and 24 weeks in the CNP and CCS, respectively. The lower cutoff in the histograms is because of our imposed 16-week lifetime threshold. These eddy lifetime estimates may underestimate the true eddy lifetimes (Chelton et al., manuscript in preparation, 2008).

[11] From Figure 1a it is clear that eddies in the CNP propagate nearly westward, while there is a preferred nonzonal orientation in the CCS. The average propagation directions are 2° south of west for the CNP and 9° south of west in the CCS.

3. A Model for Random Eddies

[12] Consider an eddy with starting location (x_j, y_j) and starting time t_j, formed in an ocean basin with zonal and meridional dimensions $[0, x_H]$ and $[y_L, y_H]$ and modeled as a westward propagating, axisymmetric Gaussian. The associated zonal geostrophic velocity field averaged over a time period T is

$$\bar{u}_j(x,y) = \frac{g}{f} \frac{a_j}{l_j}\left(\frac{y - y_j}{l_j}\right)\phi\left(\frac{y - y_j}{l_j}\right)A_j(x,T),\qquad(1)$$

where

$$A_j(x,T) = \frac{1}{T}\int_{-T/2}^{T/2}\phi\left(\frac{x - x_j}{l_j} + \frac{c_j}{l_j}\left(t - t_j\right)\right)dt,$$

$\phi(\tau) = \exp(-\frac{1}{2}\tau^2)$, a_j and l_j are the amplitude and scale of the eddy, c_j is the westward propagation speed, f is the Coriolis parameter at latitude y, and g is the gravitational acceleration. For lifetime Δ_j, the eddy does not exist for $t < t_j$ and $t > t_j + \Delta_j$. It is assumed that the eddies are evenly distributed between cyclonic and anticyclonic, so that the expected values of $\bar{u}_j$ and a_j are $E[\bar{u}_j] = E[a_j] = 0$.

[13] A realization of the time averaged zonal geostrophic velocity field is the sum of the contributions of the individual eddies: $\bar{u}(x, y) = \sum_{j=1}^{N} \bar{u}_j(x, y)$. A given set of eddies consists of N sextuplets $[x_j, y_j, t_j, a_j, l_j, \Delta_j]$, and the random function $\bar{u}(x, y)$ takes on a specific value for each location; we shall consider it to be a random function of both N and the sextuplets. The expected values of various statistics of $\bar{u}$ are found through simulation, assuming that the x_j, y_j and t_j are uniformly distributed and supposing a fixed rate of eddy production. Samples of a_j, l_j, and Δ_j are generated by bootstrapping the eddy data [Efron, 1982]. The propagation
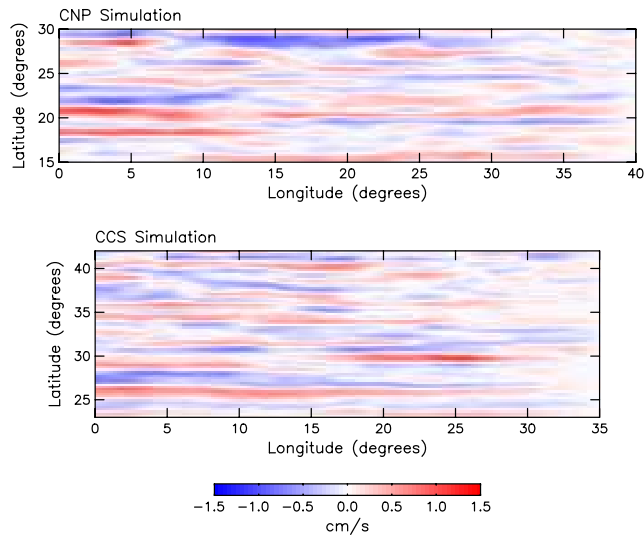
Figure 2. Representative realizations of 10-year averaged fields of simulated eddy geostrophic zonal velocity based on the eddy statistics for the (top) CNP and (bottom) CCS.

speed c_j is the long-wave baroclinic westward Rossby wave phase speed at latitude y_j that is predicted for large nonlinear eddies [*McWilliams and Flierl*, 1979].

[14] It can be shown that a good approximation for the variance of $\bar{u}$ is

$$\sigma_{\bar{u}}^2 \approx \sqrt{\pi} N^* \left(\frac{2\pi g}{fcT}\right)^2 \frac{E[a^2 l]}{2(y_H - y_L)}, \qquad (2)$$

where f and c are average values for the Coriolis parameter and the c_j, N^* is the expected number of eddies that cross any meridional section $[y_L, y_H]$ during the averaging interval $[-T/2, T/2]$, and a and l denote the random variables of eddy amplitude and scale. The normalized meridional wavenumber spectrum of $\bar{u}$ is well approximated as

$$p_{\bar{u}}(s) = \gamma E\left[a^2 l^4 e^{-(2\pi l s)^2}\right], \qquad (3)$$

where s is the meridional wavenumber and γ is chosen so that $p_{\bar{u}}$ has unit integral. To estimate equations (2) and (3), the expected values are found in the obvious way using the amplitude and scale estimates from the eddy observations. N^* in equation (2) depends on eddy lifetimes and production rate and can be estimated either directly from the eddy track data or from the empirical lifetime distributions and the properties of the uniform distribution assumed for the x_j.

4. Results

4.1. Striations

[15] Realizations of simulated $\bar{u}$ for an averaging period $T = 10$ years (Figure 2) demonstrate that the eddies do not average to zero over this time period. The obvious striations are neither jets nor preferred pathways, but the result only of random eddies. (The simulations require that eddies propagate westward, while in reality they would tend to propagate with the preferred direction for each region.)

[16] The zonal extent of these striated features is governed by the eddy speed, the lifetime distribution of the

eddies and the averaging interval *T*. Absent the constraints of *T* and the basin width, one would expect an eddy to propagate, on average, the distance covered in an average eddy lifetime. Thus as *T* increases up to the average lifetime, zonal scales should increase rapidly, and then reach a more or less steady value. For the 10-year averaging period in Figure 2, striations up to several thousand kilometers long are observed.

[17] The meridional scales of the striations in Figure 2 are quantified by the normalized power spectra calculated along $x = 0$ and ensemble averaged over 500 realizations (Figure 3a). The agreement with the analytical form (3) is very good. The striations have peak spectral energy at wavelengths of about 400 km and 250 km for the CNP and CCS, respectively. Equation (3) shows that the meridional wavenumber spectra are determined by the eddies with larger amplitudes and scales.

[18] The RMS for $\bar{u}$ obtained from the integral of the ensemble averaged meridional spectra (lower solid lines in Figure 3b) agrees well with the analytical form (2) (dotted lines). From (2), $\sigma_{\bar{u}}$ decreases as $1/T$; for a given T it depends on both the amplitude and the scale of the eddies (with larger eddies dominating), the rate of eddy production, and eddy lifetime (embodied in N^*).

[19] The simulation also affords calculation of peak-to-peak values of $\bar{u}(0, y)$ (upper solid lines in Figure 3b). The magnitudes of the eddy residuals are impressive: even 10-year averages have peak-to-peak signals of 1.6 cm s^{-1} in the CNP and 1.1 cm s^{-1} in the CCS.

[20] Our results can be compared with the striations reported by *Maximenko et al.* [2008] from 10-year averages of SSH in the CCS, which have peak-to-peak amplitudes of 0.5–1.5 cm, corresponding to geostrophic speeds of 0.3–1 cm s^{-1} at 35°N. In 10-year averages of randomly distributed eddies, we predict striations in the CCS with a peak-to-peak range of about 1 cm s^{-1}.

[21] The cross-striation wavelengths of *Maximenko et al.* [2008] are near 400 km for the CCS, longer than the 250 km we predict. On the other hand, the spectral peak in Figure 3a is broad, with significant energy at the longer wavelengths. According to (3), the spectra depend on estimates of eddy amplitude and scale, which we believe to be biased somewhat low as noted above. It is therefore likely that the true meridional spectra for eddies in this region would peak at somewhat longer scales. An estimate of the sensitivity to such a bias is available from Figures 1b, 1c, and 3a: A shift of mean amplitude and scale from 4 cm and 50 km in the CCS to 7 cm and 70 km in the CNP results in an increase of the wavelength of the spectral peak from 250 km to 400 km. Small changes in eddy amplitude and scale thus have a significant effect on the wavelength distribution of the variance.

[22] It is also noteworthy that *Maximenko et al.* [2008] apply a spatial high pass filter with spectral characteristics similar to the transfer function shown by the dashed line in Figure 3a, the result of which will be to sharpen the spectral peaks. Given the diminutive signal observed by *Maximenko et al.* [2008], our predicted signal magnitude and the breadth of the spectral peak in Figure 3a, the possibility of confounding an average of random eddies with jets is very real.
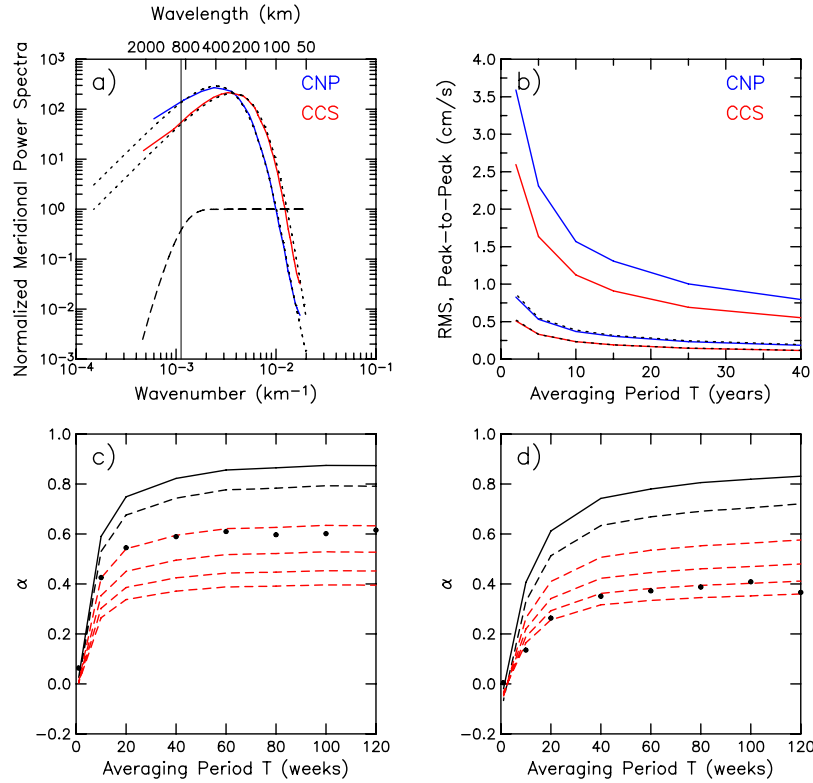
Figure 3. (a) Simulated meridional wavenumber spectra for the CNP (solid blue) and CCS (solid red) regions, along with the analytical spectra defined by equation (3) (dotted lines). The dashed line is the transfer function for a meridional high pass filter with cutoff $8°$ shown by the thin vertical line. (b) The upper pair of solid lines (blue for CNP and red for CCS) are the mean peak-to-peak values of $\bar{u}(0, y)$ in the simulations, while the lower pair are the corresponding RMS values. The dotted lines overlain on the empirically computed RMS curves show $\sigma_{\bar{u}}$ from equation (2) for the two regions. The variable α defined in the text shown as a function of averaging time T for the (c) CNP and (d) CCS. In Figures 3c and 3d, the dots show α calculated from the AVSIO SSH data, while the lines show α calculated from the random eddy model for: no noise (solid); 1 cm standard deviation errors in the SSH fields of the random eddy model (dashed); and with added isotropic signal with fractional variances of $r = 0.25, 0.50, 0.75$ and 1.0 (red dashed lines, top to bottom).

4.2. Anistropy

[23] *Huang et al.* [2007] investigated the anisotropy of time−averaged SSH fields. We calculated their spatially averaged measure of anisotropy, $\alpha = (\langle u^2 \rangle - \langle v^2 \rangle)/(\langle u^2 \rangle + \langle v^2 \rangle)$ as a function of averaging period T for the CNP and CCS regions from the SSH data (the dots in Figures 3c and 3d). Curves of α versus T computed from simulated SSH based on our random eddy model are shown by the solid lines. The discrepancies between the observations and model are similar to those found by *Huang et al.* [2007] who conclude that a simple propagating eddy model may not be sufficient to explain the behavior of α under temporal averaging.

[24] The robustness of this conclusion is sensitive to the presence of errors and isotropic, non-eddy variability in the SSH fields. Random mapping errors with 1 cm standard deviation lower the model curves (dashed lines). For isotropic non-eddy background variability with component variances $\langle \delta^2 \rangle$, the augmented anisotropy is $\alpha_\delta = (\langle u^2 \rangle - \langle v^2 \rangle)/(\langle u^2 \rangle + \langle v^2 \rangle + 2\langle \delta^2 \rangle) = \alpha/(1 + r)$, where r is the ratio of the isotropic background variance to the eddy variance. As shown by the red dashed lines, values of $r = 0.25$ and 0.75 bring the model curves into agreement with the observations in the CNP and CCS regions, respectively. We believe that there is sufficient non−eddy energy in the SSH fields to

account for values of r in this range (Chelton et al., manuscript in preparation, 2008). The larger fractional background signal required for the CCS region is not surprising given the smaller eddy amplitudes in that region compared with the CNP (Figure 1). Clearly, further studies of the noise characteristics and non-eddy variability in the observed SSH fields are necessary prerequisites to dynamical interpretation of the anisotropy in time averages.

5. Discussion

[25] We have presented a simple model for westward propagating Gaussian eddies with purely random starting locations and times. Our intention is not to represent rigorously the true eddy field, but rather to provide a "null hypothesis" that successfully mimics some features of time averages that have been interpreted as real dynamical ocean processes.

[26] This model produces striated features in time-averaged maps of zonal geostrophic velocity that, contrary to intuition, do not average rapidly to zero: the amplitude of the striations in time averages decreases only as $1/T$. The model striations are comparable in both scale and magnitude to those reported in the literature from observations and model output.

[27] The anisotropy of the time-averaged velocity fields from our simple eddy model is greater than is observed in the ocean (Figures 3c and 3d). On the other hand, we have demonstrated that the anisotropy statistic considered by *Huang et al.* [2007] is susceptible to bias induced by SSH mapping errors and isotropic signals unrelated to the eddy field. Reasonable levels of mapping error and of isotropic background variability introduce bias sufficient to resolve the discrepancy and also demonstrates the difficulty of interpreting the anisotropy of time-averaged fields.

[28] These results show that interpretation of the striations and velocity anisotropy found in time averages of observations and model output may be complicated by the presence of mesoscale eddies and other signals. Their existence does not provide unambiguous evidence of zonal jets. Following *Qiu et al.* [2008], we caution that interpretation of such results as quasi-zonal jets may be premature.

[29] On the other hand, it does appear from Figure 1a that eddies may tend to follow preferred pathways, as conjectured previously by *Maximenko et al.* [2005, 2008] and *Scott et al.* [2008]. These preferred pathways likely arise from preferred generation locations in association with permanent meanders in the CCS region [*Centurioni et al.*, 2008], and from the topographic influence of the Hawaiian Island chain on the CNP region. These mechanisms for the establishment of preferred pathways are distinctly different than spontaneous emergence from geostrophic turbulence.

References

Centurioni, L. R., J. C. Ohlmann, and P. P. Niiler (2008), Permanent meanders in the California Current System, *J. Phys. Oceanogr.*, *38*, 1690–1710.

Chelton, D. B., M. G. Schlax, R. M. Samelson, and R. A. de Szoeke (2007), Global observations of large oceanic eddies, *Geophys. Res. Lett.*, *34*, L15606, doi:10.1029/2007GL030812.

Efron, B. (1982), *The Jacknife, the Bootstrap and Other Resampling Plans*, Soc. for Ind. and Appl. Math., Philadelphia, Pa.

Huang, H.-P., A. Kaplan, E. N. Curchitser, and N. A. Maximenko (2007), The degree of anisotropy for mid-ocean currents from satellite observations and an eddy-permitting model simulation, *J. Geophys. Res.*, *112*, C09005, doi:10.1029/2007JC004105.

Maximenko, N. A., B. Bang, and H. Sasaki (2005), Observational evidence of alternating zonal jets in the world ocean, *Geophys. Res. Lett.*, *32*, L12607, doi:10.1029/2005GL022728.

Maximenko, N. A., O. V. Melnichenko, P. P. Niiler, and H. Sasaki (2008), Stationary mesoscale jet-like features in the ocean, *Geophys. Res. Lett.*, *35*, L08603, doi:10.1029/2008GL033267.

McWilliams, J. C., and G. R. Flierl (1979), On the evolution of isolated, nonlinear vortices, *J. Phys. Oceanogr.*, *9*, 1155–1182.

Qiu, B., R. B. Scott, and S. Chen (2008), Length scales of eddy generation and nonlinear evolution of the seasonally-modulated South Pacific Subtropical Countercurrent, *J. Phys. Oceanogr.*, *38*, 1515–1528.

Rhines, P. B. (1975), Waves and turbulence on a beta-plane, *J. Fluid Mech.*, *69*, 417–443.

Scott, R. B., B. K. Arbic, C. L. Holland, A. Sen, and B. Qiu (2008), Zonal versus meridional velocity variance in satellite observations and realistic and idealized ocean circulation models, *Ocean Modell.*, *23*, 102–112.

————————————
D. B. Chelton and M. G. Schlax, College of Oceanic and Atmospheric Sciences, Oregon State University, Corvallis, OR 97331, USA. (chelton@coas.oregonstate.edu; schlax@coas.oregonstate.edu)